

Chapter 2

Discrete Dislocation Dynamics: Principles and Recent Applications

2.1. Discrete Dislocation Dynamics as a link in multiscale modeling

In crystalline materials, a dislocation is a line defect which represents permanent deviations of atoms from their original crystallographic periodicity. Dislocation motion in the slip system of the crystal gives rise to macroscopic plastic deformation. A dislocation is thus a microscopic carrier of crystal plasticity.

Modeling the plasticity of crystalline materials involves understanding the nature of dislocations, which is defined at the atomistic scale and also evaluating the deformation behaviors at the macroscopic scale. Many models have been developed to understand the plasticity of metals. Since the features of plasticity vary a lot in size and time, the models also vary widely in length and time scales as depicted in Figure 2.1. Out of a range of models, most attention is given in this chapter to Molecular Dynamics (MD), Dislocation Dynamics (DD) and Continuum Mechanics (CM) with a special emphasis on DD simulations.

Atoms are the basic constituent elements of MD simulations. Atoms interact with each other through interatomic potentials. The temporal trajectory of a set of atoms under an external loading is simulated by minimizing the total potential energy of the system. The deviations of the position of the atoms from the lattice sites implicitly represent the dislocations. The atomistic scale topology of a dislocation line can thus be investigated by MD. MD simulations are employed

mostly in studying physical properties of a single or a few dislocation lines due to the constraints of the simulation size ($<(200 \text{ nm})^3$).

In DD methods, dislocation lines are represented explicitly. Each dislocation line is treated as an elastic inclusion embedded in an elastic medium. The collective evolution of a large number of interacting dislocations under an external loading is simulated using elastic properties of the crystal. Core properties of dislocations such as line mobility, junction strength etc., are input parameters of DD simulations that can be derived from MD simulations. DD simulations give access to the dislocation patterning but also to the mechanical response of the simulated volume ($<(50 \mu\text{m})^3$).

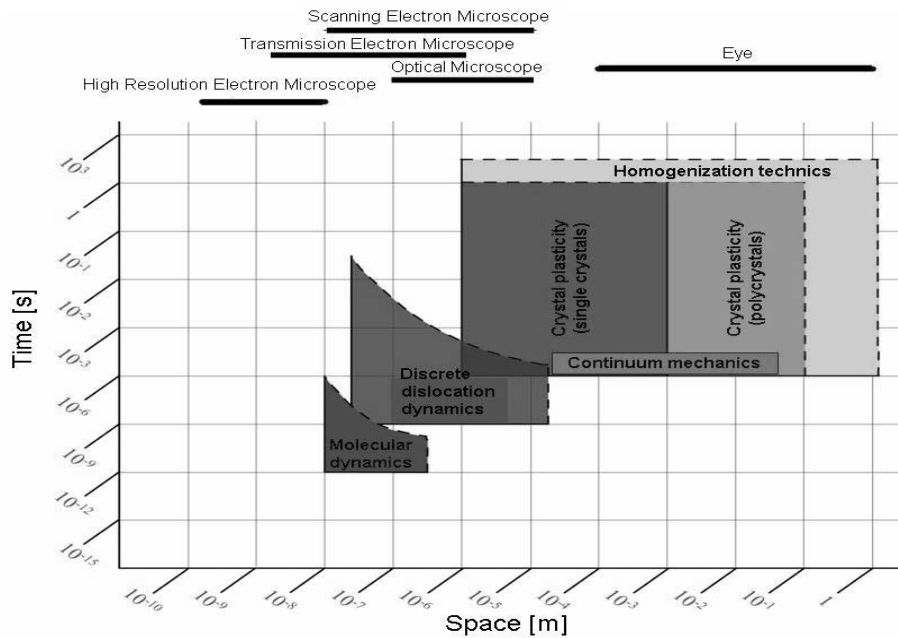


Figure 2.1. Typical volume size and physical time covered by three models devoted to crystal plasticity

At a higher scale, CM treats the behavior of a continuum medium using a set of equations and boundary conditions. There is a wide range of numerical techniques which can solve the equations. Finite difference and finite element methods are two broad subsets of such techniques. In these methods, a continuum domain of interest is subdivided into discrete cells or elements, in which the values of certain physical quantities are determined by solving a system of equations. Ideally, CM should use a set of constitutive equations that accurately account for the physics at the origin of

the plasticity which, in the case of crystalline materials is closely related to the dislocation dynamics. Thus, DD simulations can obviously feed CM models by calculating the constitutive equations. In CM, the maximum size of the simulated volume is not limited but instead imposed by the space resolution associated with the problem treated. However, each simulation cell must be big enough to be representative of a continuum medium in agreement with the constitutive equations.

As introduced briefly above, MD, DD and CM have their own characteristic length and time scale. Figure 2.1 shows such ranges of length and time scales for each method. As the performance of each numerical method is improved, the volume and the physical time which can be simulated increase (top and right domain limits of each method in Figure 2.1). Recently the length and time scales of the three methods begin to overlap. This gives a great impetus to exchange information between the different models in order to build up a unified description of crystal plasticity, which would ideally be able to predict the behavior of a material from the fundamental properties of the atoms.

2.2. Principle of Discrete Dislocation Dynamics

The concept of 3D discrete dislocation simulations was imagined by L. Kubin, Y. Bréchet and G. Canova in the early 1990s [KUB 92], [DEV 92]. The first code *Micromégas* was a simple model for which dislocation lines of a f.c.c. single crystal are sub-divided into sets of edge and screw dislocation segments embedded in a continuum medium as pictured in Figure 2.2a.

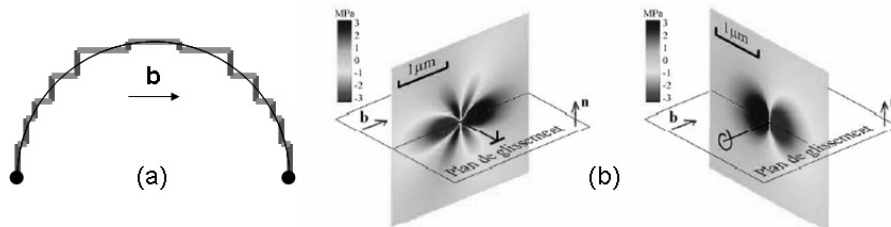


Figure 2.2. (a) Edge-screw discretization of dislocation lines; (b) internal stresses induced by edge and screw segments

Each dislocation segment generates a long range elastic stress field within the entire simulated sample. In the case of isotropic elasticity, analytical expressions for the internal stress generated by a finite segment have been established by J.C.M. Li [LI 64] and R. DeWit [DeWIT 67]. Taking into account the anisotropy of the elastic

medium is more challenging in term of calculation time since there is no explicit relationship. We can however use the line integrals proposed by J. Willis [WIL 70].

Using linear elasticity properties, the effective stress applied on each dislocation is evaluated at the middle point of each segment as the superposition of the internal stress induced by all the segments in the simulated volume and the applied stress imposed by the loading. This induces a force given by the Peach-Koehler equation

$$\mathbf{F} = (\boldsymbol{\sigma}_{\text{int}} + \boldsymbol{\sigma}_{\text{app}}) \mathbf{b} \times \boldsymbol{\xi} \quad [2.1]$$

where $\boldsymbol{\xi}$ is the unit vector of the line direction and \mathbf{b} the Burgers vector of the dislocation segment. In DD simulations, most of the CPU time is devoted to evaluating equation [2.1] since this implies N^2 computations of the internal stress tensors, and the number of segments, N , continuously increase with time. Thus, many efforts have been carried out in optimizing the calculation of the internal stresses. As an example, Bulatov *et al.* recently proposed a fast multipole decomposition leading to N operations [CAI 06]. These optimizations can still be improved by using parallel calculation which is now a common option in most DD codes [SCH 99] [SHI 06] [ARS 07].

Once the force is known on each dislocation segment, the segments are displaced according to mobility functions which depend on the material properties. In the case of FCC structure, the velocity is a linear function of the glide component of the force whereas in the case of materials with large Peierls valleys, like BCC for example, the velocity of screw segments is given by a thermally activated relationship using a Boltzman relation [TAN 98] [CHA 06].

Typical outputs of DD simulations are obviously the dislocation microstructure but also much statistical data such as the dislocation densities, the cumulated shear strain, the stored energy, the local stresses, etc. Recently, methods have been developed in order to calculate the actual shape of any part of the crystal deformed by the dislocations as illustrated in Figure 2.3.

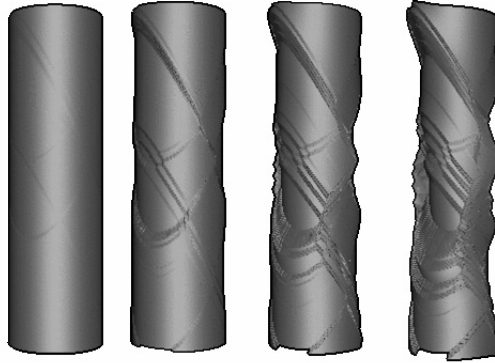


Figure 2.3. *Example of calculation of the actual shape of a crystal deformed by dislocation activity. Case of a copper single crystal loaded in uniaxial tension along (112) axis*

From some points of view, DD simulations can be seen as an ideal tool to fill the gap between atomic simulations (MD) and continuum modeling. These properties explain the large dissemination of this modeling during the past few years. Today, there are more than a dozen discrete dislocation dynamics codes throughout the world [ZBI 98] [SCH 99] [GHO 00] [WEY 02] [BUL 06] dedicated to different crystallographic structures but all based on similar ingredients. The studies presented hereafter have all been performed using the code `Tridis` developed in Grenoble, France [VER 98].

2.3. Example of scale transition: from DD to Continuum Mechanics

2.3.1. Introduction to a dislocation density model

The development of constitutive equations for crystal plasticity is still challenging today. The objective is always to derive a set of behavior laws including most of the physics involved during plastic deformation. In the case of crystalline materials, this involves accounting for dislocation properties at the continuum scale.

In this section, we present a crystal plasticity model for which the dislocation densities on the different slip systems are the internal variables. Three equations are needed to relate the stress to the plastic strain. We should note that each law is derived from physical considerations of dislocation motions.

2.3.1.1. Constitutive equations of a dislocation based model of crystal plasticity

Plastic behaviors of crystals have been studied since the early 1960s [TEO 75]. Let us consider the motion of a single dislocation gliding on slip system s and embedded in a heterogenous stress field. Assuming that the dislocation motion is governed by the obstacles (as usually admitted for FCC structures), these obstacles can be classified in two categories:

- (i) obstacles inducing long-range stresses τ_μ like for example dislocations stored at grain boundaries or around precipitates;
- (ii) obstacles inducing a short-range stress field, written as τ^* , like in the case of forest dislocations or impurities.

τ_μ does not depend on temperature whereas τ^* is thermally activated. Following this distinction, we can define a typical spatial evolution for the stress component as plotted in Figure 2.4.

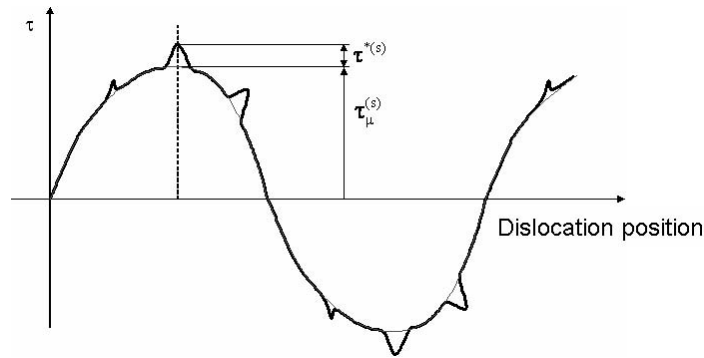


Figure 2.4. Decomposition of the stress fields felt by a moving dislocation at a given temperature

When considering only the isotropic hardening, the spatial evolution of the athermal stress τ_μ is similar to a periodic function with a zero average and a large wavelength. When a dislocation meets an obstacle which acts within few atomic distances to the dislocation position, it needs an additional stress τ^* to pass the obstacle. For each slip system s , the resolved shear stress needed for the dislocation motion is then

$$\tau^s = \tau_\mu^s + \tau^{*s} \quad [2.2]$$

When the time for the dislocation flight is negligible in comparison to the waiting time in front of the obstacle, we can write the following expression for the dislocation velocity [TEO 76]:

$$v = \frac{bv_D}{\exp\left(\frac{\Delta G_0}{kT}\right)} 2\text{sh}\left(\frac{\tau^{*s}\Delta V^*}{kT}\right) \quad [2.3]$$

where v_D is the Debye frequency, b the Burgers vector magnitude, ΔG_0 and ΔV^* the activation energy and activation volume respectively.

Averaging the velocities out of the whole mobile dislocation density ρ_m of a given slip system is achieved using the Orowan equation:

$$\dot{\gamma}^s = \rho_m b \bar{v} \quad [2.4]$$

When the effective resolved shear stress is moderate (less than 70% of the value at 0 K, we can neglect the inverse probability so that the sinh in equation [2.4] is replaced by the negative exponential part. Replacing $\tau^{*(s)}$ by $(\tau_\mu^{(s)} - \tau^{(s)})$, the first order approximation in terms of $\tau^{(s)}/\tau_\mu^{(s)}$ finally gives [RAU 93]:

$$\dot{\gamma}^{(s)} = \rho_m^{(s)} b^2 v_D \exp\left(\frac{-\Delta G_0}{kT}\right) \left(\frac{\tau^{(s)}}{\tau_\mu^{(s)}}\right)^{\frac{\tau_\mu^{(s)}\Delta V^*}{kT}} = \dot{\gamma}_0^{(s)} \left(\frac{\tau^{(s)}}{\tau_\mu^{(s)}}\right)^n \quad [2.5]$$

Equation [2.5] is the flow law written under the classic form of a power relationship between strain rate and normalized stress.

Let us briefly recall the assumptions needed to establish this equation. Equation [2.5] is valid for moderate values of $\tau^{(s)}$. Moreover, the first order approximation implies that $\tau^{(s)} \ll \tau_\mu^{(s)}$. These conditions are fulfilled for most FCC metals within a range of temperatures lower than $0.3 T_f$, (so-called cold regime of deformation). Parameters $\dot{\gamma}_0^{(s)}$ and n have been established from an average performed over all the mobile dislocations within a given slip system so that the three macroscopic variables $\tau^{(s)}$, ΔG_0 and ΔV^* are now pseudo-phenomenological constants although the underlying physics is still there. In other words, this means that we need to identify the value of these parameters.

Strain hardening is defined by the increase of the athermal stress $\tau_\mu^{(s)}$ with the internal variables, i.e. the dislocation densities. Such a relationship is introduced through the Mecking and Kocks equation [MEC 81]:

$$\tau_{\mu}^{(s)} = \alpha \mu b \sqrt{\rho_F} \quad [2.6]$$

where ρ_F is the forest dislocation density and α a coefficient close to 0.3. This equation can be split over the 12 slip systems of the FCC crystal using a matrix a which corresponds to the slip system interactions.

$$\tau_{\mu}^{(s)} = \mu b \sqrt{\sum_{u=1}^{12} a_{su} \rho^{(u)}} \quad [2.7]$$

The closed form of the system of constitutive equations is obtained by the writing the evolution of the dislocation density with the deformation. The relationship can be explained from statistical considerations of dislocation production and annihilation [MEC 81] [ESS 79].

$$\dot{\rho}^{(s)} = \frac{1}{b} \left(\frac{\sqrt{\sum_{u=1}^{12} d_{su} \rho^{(u)}}}{K} - 2\beta R \rho^{(s)} \right) \dot{\gamma}^{(s)} \quad [2.8]$$

This equation involves a storage term with a mean free path of the form $\Lambda = K/\sqrt{\rho}$ and an annihilation term based on the annihilation distance $y_c = \beta R$. Equation [2.7] implies that dislocation densities will saturate when the production term equals the annihilation term leading to a saturation of the isotropic hardening.

Finally, the crystal plasticity model is defined by the set of three equations [2.5], [2.7] and [2.8]. They can be rewritten in a classical form by calculating the derivative of [2.7] and introducing $\dot{\rho}^{(s)}$ given by [2.8]. This gives:

$$\dot{\tau}_{\mu}^{(s)} = \sum_{u=1}^{12} \left\{ \frac{\mu a_{su}}{2 \sqrt{\sum_{p=1}^{12} a_{sp} \rho^{(p)}}} \left(\frac{\sqrt{\sum_{q=1}^{12} d_{uq} \rho^{(q)}}}{K} - 2\beta R \rho^{(u)} \right) \dot{\gamma}^{(u)} \right\} \quad [2.9]$$

Note that these constitutive equations are only valid for monotonic loading since they do not account for any kinematic hardening.

2.3.1.2. Parameter identification

The DD model presented in section 2.2 is well adapted to identify the coefficients involved in this dislocation density-based model of crystal plasticity. As an example, any a_{su} coefficient of the hardening law can be determined by

simulating the interaction of slip systems (s) and (u) and measuring the shear stress applied on system (s) needed to force it to cross the population of dislocation on forest system (u) of density $\rho^{(u)}$ [FIV 97]. Following this idea, we can identify the 12x12 coefficients of matrix a (which is restricted to 5 independent values depending on the 3D geometry of the system interaction a_1^{copla} , a_1^{ortho} , a_1^{coli} , a_2 , a_3). Recently, Devincere *et al.* [DEV 06] found the following values for copper single crystals: $a_1^{\text{coli}}=0.625 \pm 0.044$; $a_3=0.122 \pm 0.012$; $a_2=0.137 \pm 0.014$; $a_1^{\text{copla}} \approx a_1^{\text{ortho}}=0.0454 \pm 0.003$.

Similarly, it is possible to measure the values of coefficients K and y_c from DD curves giving the evolution of the dislocation densities on the different slip systems with the plastic deformation [FIV 98] [TAB 98].

For copper, we find a typical value $K=32$ for the mean free path and $y_c=3.b$ for the annihilation distance.

2.3.1.3. Application to copper simulations

The constitutive equations are easily introduced in a finite element code such as ABAQUS using the User MATerial routines. Using the parameters identified by DD simulations, we can now simulate the visco-plastic behavior of any single crystal under a given loading. Note that polycrystalline materials can also be simulated provided the mean free path involved in equation [2.8] is modified in order to account for the distance between the integration Gauss point and the grain boundary.

Figure 2.5 shows the simulation of a copper single crystal loaded in tension along the $(\bar{1}25)$ direction.

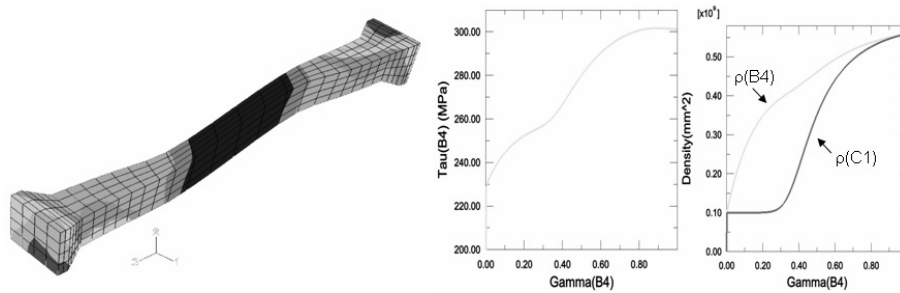


Figure 2.5. Simulation of a tensile test along $(\bar{1}25)$

Initially, the Schmid factor is the highest on system B4: $(111)[\bar{1}01]$. This corresponds to stage I where the hardening rate is weak since there is only a single

slip system activated. If rotations are allowed in the grips as shown in the deformed mesh plotted in Figure 2.5, the Schmid factor changes with the plastic deformation cumulated in system B4. This activates a secondary slip system C1: $(11\bar{1})[011]$. Dislocation activity in system B4 is then modified by the forest dislocations of system C1 so that the hardening rate is more pronounced. This is the stage II regime. Finally, as soon as the two dislocation densities are closer to the saturation value, the stress tends to saturate so that the hardening rate decreases in the so-called stage III.

2.3.1.4. Taking into account kinematic hardening

Fatigue simulations performed in DD (see section 2.4) revealed the effect of dipole interactions on the mechanical response of a single crystal of copper submitted to a cyclic loading. This gave information on the intra-granular hardening and more precisely on the kinematic part of the hardening, i.e. the hardening stress which can be recovered when the loading is reversed. This section presents a model that can reproduce most of the experimental features of fatigue [DEP 08]. The model is based on dipole interactions and can nicely complete the set of constitutive equations presented in section 2.3.1. It can be shown from dislocation theory [HIR 82], [FRI 64] that a dipole of height h has a strength s written as

$$s = \frac{\mu b}{8\pi(1-\nu)h} \quad [2.10]$$

The distance h is easily estimated from DD simulations. Figure 2.6a shows a typical dislocation microstructure within a grain cyclically loaded in pure shear with a plastic strain amplitude $\Delta\gamma_p = 3 \cdot 10^{-3}$. The distribution of the dipole heights is reported in Figure 2.6b.

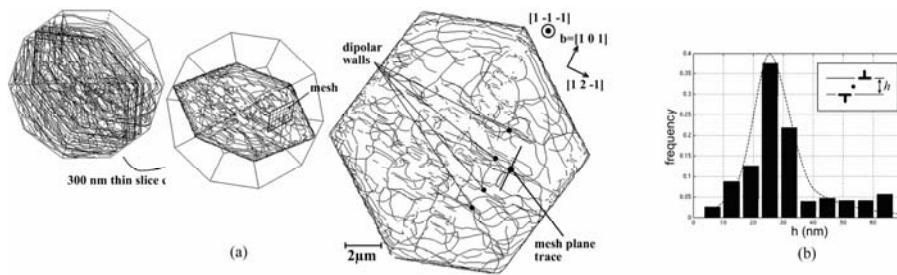


Figure 2.6. Thin foil taken out from a DD fatigue simulation and distribution of dipole heights

Assuming that the height distribution follows a Gaussian function, experiments show that the mean value evolves as $1/\sqrt{\rho}$ [CAT 05] so that the distance decreases when the dislocation density increases. The corresponding dipole strength can now be calculated using equation [2.10] as shown in Figure 2.7 for two values of the dislocation density in the DD simulation.

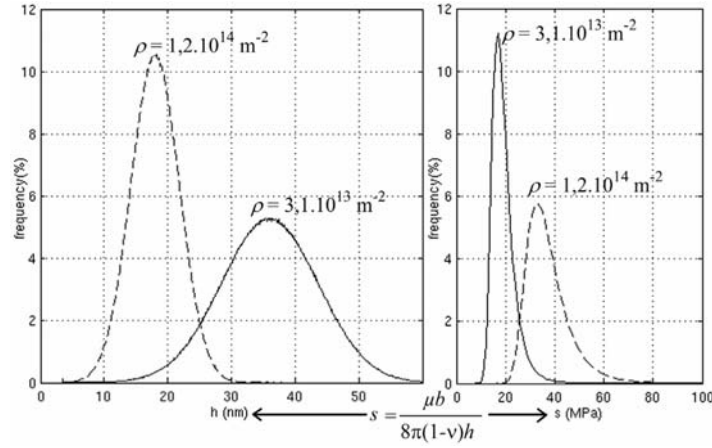


Figure 2.7. Distribution of the dipole height and corresponding dipole strength calculated for two values of the dislocation density

For the sake of simplicity, we will assume that the strength distribution also fits a Gaussian function $f(s)$ defined by the average value \bar{s} and the standard deviation σ_s :

$$\bar{s} = \int_0^{\infty} sf(s)ds = \tau_0 + \alpha Gb\sqrt{\rho} \quad ; \quad \sigma_s = \sqrt{\int_0^{\infty} (s - \bar{s})^2 f(s)ds} = \lambda \bar{s} \quad [2.11]$$

As shown in equation [2.11], the average value is supposed to be proportional to the dislocation density via a classical relationship proposed by Mughrabi [MUG 75]. Moreover, experiments show that the standard deviation is proportional to the average value using a constant coefficient λ [CAT 05]. This behavior was recently confirmed by DEPRES using DD simulations [DEP 04].

Locally, the stress may destabilize the weakest dipoles which can then contribute to the shear strain rate as:

$$\dot{\gamma}_s = \dot{\gamma}_0 \left| \frac{\tau - X}{s} \right|^{1/m} \text{sign}(\tau - X) \quad [2.12]$$

where X is a long range internal stress induced by the strain gradients. The displacements induced by the dislocation on the grid located in Figure 2.6 point out these gradients. The corresponding deformed mesh is plotted in Figure 2.8. The three marks indicate that extra dislocations are located between marks 1 and 2 and also between marks 2 and 3.

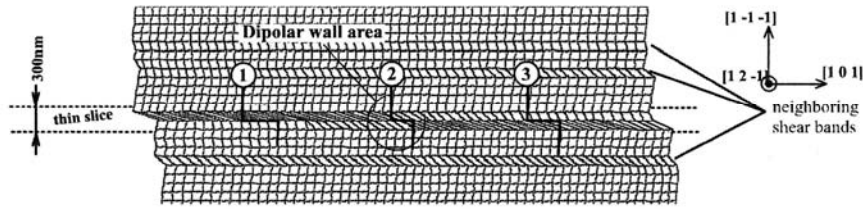


Figure 2.8. Evidence of extra dislocations inducing strain gradients

These excess dislocations (often called geometrically necessary dislocations) are all pinned on dipoles. Thus, they induce a back stress on the source from which they have been emitted. This kinematic back stress can be roughly estimated as the stress induced by an equivalent dislocation loop of radius \bar{r} with a net Burgers vector Nb . The number of loops N is directly related to the difference between the local deformation at the dipole location and the macroscopic strain γ : $N=(2R/b)(\gamma-\gamma_s)$. Thus, the back stress, X is given as $X=ANG/2\bar{r}$ where A is a geometric parameter depending on the actual geometry of the grain and the dislocation loops. Replacing N by its dependence over the shear strain, we finally obtain:

$$X = AG \frac{R}{\bar{r}} (\gamma_s - \gamma) = MG(\gamma_s - \gamma) \quad [2.13]$$

DD simulation shows that the geometric coefficient M is close to a constant $M \approx 2$. Equation [2.11] can now be introduced in equation [2.12] in order to define a new flow law accounting for kinematic hardening.

The constitutive model based on equation [2.11], [2.12], [2.13] can be completed by dislocation evolution law [2.8] so that it can be used to derive the mechanical response of a grain submitted to a cyclic loading. A typical response is given in Figure 2.9 together with the experimental results of Mughrabi [MUG 78]. Numerical results were obtained with $M=2$ and $\lambda=0.8$.

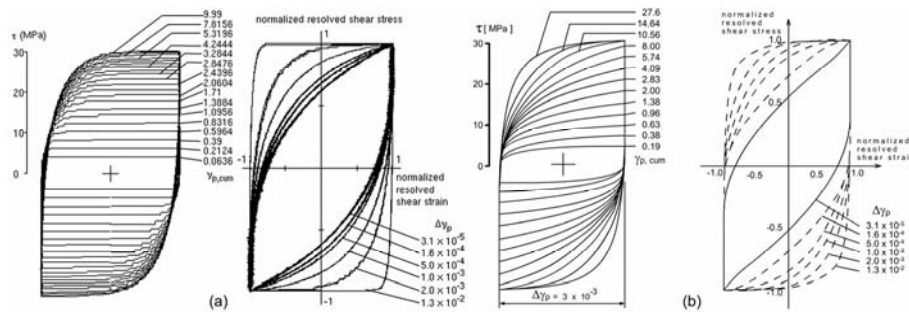


Figure 2.9. (a) Predicted hysteresis loops for a given imposed plastic strain amplitude $\Delta\gamma_p = 3.10^{-3}$ and loop shape obtained for different imposed strain amplitudes; (b) corresponding experiments published by Mughrabi [MUG 78]

The proposed model is in very good agreement with the experimental measurements of Mughrabi, both for the evolution of the hysteresis at a given imposed strain amplitude and also for the shape of the cycle reached at saturation for different strain amplitudes. To conclude this part on the kinematic hardening, let us recall that the proposed model only adds 2 constants M and λ to the original isotropic hardening model. Here, a simple scalar model is presented but it can easily be written in a tensor manner and implemented in finite elements to treat any complex path loading.

2.4. Example of DD analysis: simulations of crack initiation in fatigue

2.4.1. Case of single phase AISI 316L

In power plants, AISI 316L stainless steel is usually used in the internal parts of the cooling systems. When subjected to thermal fatigue, as in the case of the injection of a cold fluid in the circuit, transgranular fatigue cracks are observed. In order to study the crack formation, the CYTHIA experiment (CYclage THERmique par Induction des Aciers) has been conceived at Commissariat à l'Énergie Atomique (CEA/SRMA). This ideal experiment consists of cyclically heating a pipe using a high frequency induction coil whereas the inner part of the pipe is constantly cooled by flowing water. Transmission Electron Microscopy (TEM) observations of the surface grains located at the outer part of the cylinder show a dense dislocation microstructure organized in bands typical of fatigue behavior of this type of material [MUG 92], [LI 94], [OBR 94]. Atomic Force Microscopy (AFM) observations of the grain surface show that with the cycles, the persistent slip bands lead to the development of extrusion and intrusion relief at the surface [MAN 02], [MAN 03] that may induce cracks.

Many DD simulations with various conditions of loading amplitude and grain size were performed with a view to explain both the formation of the persistent slip bands [DÉP 04b] and the relationship with the surface relief and the nucleation of the first crack [DÉP 06]. As shown in Figure 2.10, the simulation volume corresponds to an isolated grain with one free surface. The applied loading is assumed homogenous within the entire grain and the grain boundaries are treated as impenetrable obstacles to the dislocation motion. For all the simulations the plastic strain amplitude is imposed and only two glide systems sharing the same Burgers vector are considered. The initial dislocation configuration consists of a single dislocation source whose characteristics are given by the TEM observations performed on CYTHIA samples: the Burgers vector is nearly aligned with the vector normal to the surface. Both pure shear and double glide loading conditions have been tested.

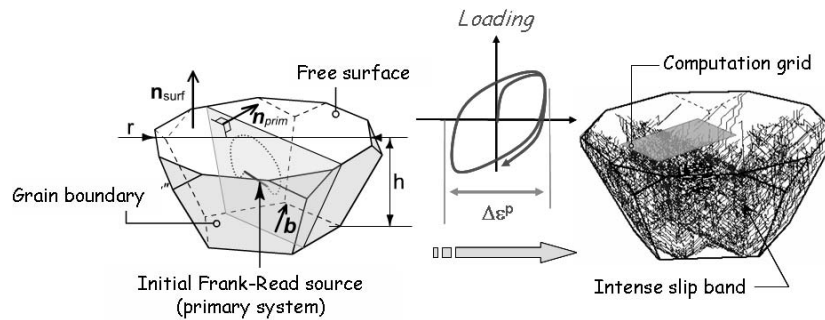


Figure 2.10. Initial configuration of the dislocation simulation and typical dislocation microstructure obtained after 25 cycles performed with imposed plastic strain amplitude

It was found that the cross-slip mechanism plays a crucial role in the organization of the dislocation microstructure [DÉP 04b]. First, it allows dislocations to invade the whole grain leading to a beneficial homogenization within the simulated volume of the plasticity. Then the numerous reactions of the dislocation lines on the two interacting slip systems lead to the formation of intense slip bands as shown in Figure 2.10. DD simulations explained in detail the mechanism at the origin of this typical dislocation organization. After a few cycles, edge dipoles are formed in the so-called vein structures and when dislocations from the cross-slipped system shear these zones, the dislocation lines recombine and form a complex microstructure containing channels, entangled zones and piled-up dislocations as depicted in Figure 2.11 below.

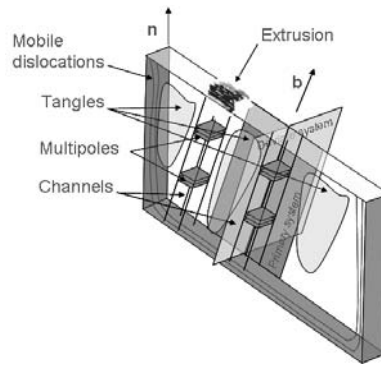


Figure 2.11. Schematic description of a persistent slip band as observed in DD simulations

The dislocations within the channels consist of multipoles made of prismatic loops and helicoidal dislocations. The density of multipoles continuously increases with the cycles, storing more and more energy in the band. Note that the mobility of these dislocations is restricted to a cylinder defined by the loop size and the Burgers vector. Under a homogenous stress field, the multipoles cannot move. Inversely, when submitted to a stress gradient, they can glide in the channel and possibly reach the surface where interstitial loops print tongue-like extrusions and vacancy loops leave a punch in the surface (intrusion) as shown in Figure 2.11.

Complementary analyses of the surface relief were performed when the imposed plastic strain is at maximum. It was shown that all the plasticity is localized at the interface between the slip band and the matrix. At this place are located highly mobile dislocations (see Figure 2.10) which completely accommodate the imposed plasticity. Note that such dislocations are hardly observed in microscopy since observations are usually performed *post mortem* and only a few experiments are carried out *in situ* [LEP 85]. When these dislocations move, they induce a stress gradient on the multipoles which drive them out of the volume.

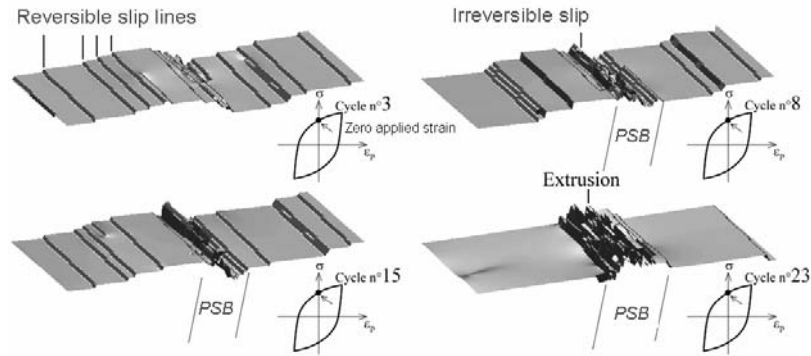


Figure 2.12. Evolution of the surface relief with the cycles. The computation is performed on the grid indicated in Figure 2.10

The crack nucleation was studied by calculating both the energy and the stress state in the bands. As discussed previously, the multipoles store energy in the band with the cycles. However, DD simulations show that the stress component needed to open a crack is saturated after a few cycles. This means that a crack can not initiate inside the bands but rather at the surface where the stress is concentrated by the extrusion/intrusion shape of the surface relief. From a simulation campaign performed with different values of the plastic strain amplitude, the mean strain, the grain size, the grain shape and the stress triaxiality, it was possible to derive the effect of these parameters on the fatigue life [DEP 06]. It was found that the extrusion growth is a linear function of the strain range and grain size and evolves as a square root function of the number of cycles. When comparing these predictions of the extrusion growth rate with the experimental measures [MAN 03], [MAN 02], we can note a good agreement for the first few cycles and a discrepancy for the large number of cycles. The difference can be attributed to diffusion of point defects that could change the square-root relationship into a linear form. Despite this limit, the predictions derived from the DD simulations are of great interest since the experiments show that the crack always initiates very early in the cycling process, i.e. where the DD prediction is relevant.

2.5. Conclusions

This chapter presented two studies involving discrete dislocation dynamics simulations. In the first example the DD code was used to identify constitutive equations of a continuous model of crystal plasticity. The model being based on dislocation densities, quantities were calculated by DD simulations and a complete

visco-plastic model of a FCC crystal taking into account both isotropic and kinematic hardening was proposed.

The second example concerned a study of crack initiation in fatigue where DD simulations explained the formation of the dislocation microstructure into the typical persistent slip bands observed in experiments. It was shown that the extrusion printed at the surface of a grain stressed in fatigue can be obtained with dislocation motions. There is no need to account for a non-conservative mechanism such as diffusion of point defects. Finally, a prediction of the fatigue life was obtained through a simulation campaign of DD simulations.

In many cases, DD simulations need information from a lower scale in order to specify local rules that cannot be fulfilled by elastic theory. As an example, the dislocation mobility in BCC materials is related to the core of the dislocations. Such information can be obtained from atomic simulations [CHA 06]. Then DD simulations can be used to analyze the collective effect of a large population of dislocations and fill the gap between atomic and continuum scales.

2.6. Bibliography

- [ARS 07] ARSENLIS A., CAI W., TANG M., RHEE M., OPPELSTRUP T., HOMMES G., PIERCE T.G., BULATOV V.V., “Enabling strain hardening simulations with dislocation dynamics”, *Modelling Simul. Mater. Sci. Eng.*, 15, pp. 553-595, 2007.
- [BAR 85] BARNETT D.M., “The displacement field of a triangular dislocation loop”, *Phil. Mag.*, 28(3), pp. 383-387, 1985.
- [BUL 06] BULATOV V.V., CAI W., *Computer simulations of dislocations*, Oxford University Press, A.P. Sutton and R.E. Rudd, 2006, 352 pages.
- [CAI 06] CAI W., ARSENLIS A., WEINBERGER C., BULATOV V.V., “A non-singular continuum theory of dislocations”, *J. Mech. Phys. Solids*, 54, pp. 561-587, 2006.
- [CAT 05] CATALAO S., FEUGAS X., PILVIN P., CABRILLAT M.T., “Dipole heights in cyclically deformed polycrystalline AISI 316l stainless steel”, *Mater. Sci. Eng. A*, 400-401, p. 349, 2005.
- [CHA 06] CHAUSSIDON J., FIVEL M., RODNEY D., “The glide of screw dislocations in bcc fe: atomistic static and dynamic simulations”, *Acta Mater.*, 54, pp. 3407-3416, 2006.
- [DÉP 04] DÉPRÉS C., Modélisation physique des stades précurseurs de l’endommagement en fatigue dans l’acier inoxydable austénitique 316L, Thesis, INP Grenoble, 2004.
- [DÉP 04b] DÉPRÉS C., ROBERTSON C., FIVEL M.C., “Low-strain fatigue in aisi 316l steel surface grains: a three-dimensional discrete dislocation dynamics modelling of the early cycles Part I: Dislocation microstructures and mechanical behaviour”, *Phil. Mag.*, 84, no. 22, pp. 2257-2275, 2004.

- [DÉP 06] DÉPRÉS C., ROBERTSON C., FIVEL M.C., “Low-strain fatigue in 316l steel surface grains: a three dimension discrete dislocation dynamics modelling of the early cycles. part 2: Persistent slip markings and micro-crack nucleation”, *Phil. Mag.*, 86(1), pp. 79-97, 2006.
- [DÉP 08] DÉPRÉS C., FIVEL M., TABOUROT L., *Scripta Mater.*, “A dislocation-based model for low-amplitude fatigue behaviour of face-centred cubic single crystals”, *Scripta Mater.*, 58(12), pp. 1086-1089, 2008.
- [DEV 06] DEVINCRE B., KUBIN L., HOC T., “Physical analyses of crystal plasticity by DD simulations”, *Scripta Mater.*, 54, pp. 741-746, 2006.
- [DEV 92] DEVINCRE B., PONTIKIS V., BRECHET Y., CANOVA G., CONDAT M., KUBIN L.P., *Three-dimensional Simulations of Plastic Flow in Crystals*, Plenum Press: New York, M. Marechal, B.L. Holian (eds.), 1992, p. 413.
- [DeWIT 67] DEWIT R., “Some relations for straight dislocations”, *Phys. Stat. Sol.*, 20, pp. 567-573, 1967.
- [ESS 67] ESSMANN U., MUGHRABI H., “Annihilation of dislocations during tensile and cyclic deformation and limits of dislocation densities”, *Phil. Mag. A*, 40(6), pp.731-756, 1979.
- [FIV 97] FIVEL M., Etudes numériques à différentes échelles de la déformation plastique des monocristaux de structure cfc, Doctoral thesis, Institut National Polytechnique de Grenoble, 1997.
- [FIV 98] FIVEL M., TABOUROT L., RAUCH E., CANOVA G., “Identification through mesoscopic simulations of macroscopic parameters of physically based constitutive equations for the plastic behaviour of fcc single crystals”, *J. Phys. IV*, 8(Pr 4), pp. 249-258, 1998.
- [FRI 64] FRIEDEL J., *Dislocations*, Oxford, Pergamon Press, 1964.
- [GHO 00] GHONIEM N.M., TONG S.-H., SUN L.Z., “Parametric dislocation dynamics: a thermodynamics-based approach to investigations of mesoscopic plastic deformation”, *Phys. Rev. B*, 61(1), pp. 1-15, 2000.
- [HIR 82] HIRTH J.P., LOTHE J., *Theory of Dislocations*, 2nd edition, New York: McGraw-Hill, Wiley Interscience, 1982.
- [KUB 92] KUBIN L.P., CANOVA G.R., “The modelling of dislocation patterns”, *Scripta Metall.*, 27, pp. 957-962, 1992.
- [LEP 85] LEPINOUX J., KUBIN L.P., “*In situ* TEM observations of the cyclic dislocation behaviour in persistent slip bands of copper single crystals”, *Phil. Mag. A*, 51(5), pp. 675-696, 1985.
- [LI 64] LI J.C.M., “Stress field of a dislocation segment”, *Phil. Mag.*, 10, pp. 1097-1098, 1964.
- [LI 94] LI Y., LAIRD C., “Cyclic response and dislocation structures of aisi 316l stainless steel. part 1: single crystals fatigued at intermediate strain amplitude”, *Mater. Sci. Eng. A*, A186, pp. 65-86, 1994.

- [MAN 02] MAN J., OBRTLÍK K., BLOCHWITZ C., POLÁK J., “Atomic force microscopy of surface relief in individual grains of fatigued 316l austenitic stainless steel”, *Acta Mater.*, 50, pp. 3767-3780, 2002.
- [MAN 03] MAN J., OBRTLÍK K., POLÁK J., “Study of surface relief evolution in fatigued 316l austenitic stainless steel by AFM”, *Mater. Sci. Eng. A*, 351, pp. 123-132, 2003.
- [MEC 70] MECKING H., LÜCKE K., “A new aspect of the theory of flow stress in metals”, *Scripta Metall.*, 4(6), pp. 427-432, 1970.
- [MEC 81] MECKING H., KOCKS U.F., “Kinetics of flow and strain hardening”, *Acta Metallurgica*, 29, pp. 1865-1875, 1981.
- [MUG 75] MUGHRABI H., “Description of the dislocation structure after unidirectional deformation at low temperature”, *Constitutive Equations in Plasticity*, Cambridge Massachussetts, p. 199-250, 1975.
- [MUG 78] MUGHRABI H., “The cyclic hardening and saturation behaviour of copper single crystals”, *Mater. Sci. Eng. A*, 33(2), pp. 207-233, 1978.
- [MUG 92] MUGHRABI H., “Introduction to the viewpoint set on: surface effects in cyclic deformation and fatigue”, *Scripta Metall. Mater.*, 26, pp. 1499-1504, 1992.
- [OBR 94] OBRTLÍK K., KRUML T., POLÁK J., “Dislocation structure in 316l stainless steel cycled with plastic strain amplitudes over a wide interval”, *Mater. Sci. Eng. A*, A187, pp. 1-9, 1994.
- [RAU 93] RAUCH E., Etude de l'écroutissage des métaux : Aspects microstructuraux et lois de comportement, Thesis, Institut National Polytechnique de Grenoble, 1993.
- [SCH 99] SCHWARZ K., “Simulation of dislocations on the mesoscopic scale. i. methods and examples”, *J. Appl. Phys.*, 85(1), pp. 108-119, 1999.
- [SHI 06] SHIN C.S., FIVEL M.C., VERDIER M., OH K.H., “Numerical methods to improve the computing efficiency of discrete dislocation dynamics simulations”, *J. of Comp. Phys.*, 215(2), pp. 417-429, 2006.
- [TAB 98] TABOURET L., FIVEL M., RAUCH E., “Use of mesoscopic simulations to model the dislocation densities evolution law”, *Proceedings of the 19th Riso International Symposium on materials Science*, Winther G., Cartensen J.V., Leffers T., Lorentzen T., Pedersen O.B., Sorensen B.F. (eds.), pp. 511-516, Riso National Laboratory, Roskilde, Denmark, 1998.
- [TAN 98] TANG M., KUBIN L.P., CANOVA G.R., “Dislocation mobility and the mechanical response of bcc (ta) single crystals: a mesoscopic approach”, *Acta Metall. Mater.*, 46(9), pp. 3221-3235, 1998.
- [TEO 75] TEODOSIU C., “A physical theory of the finite elastic-viscoplastic behaviour of single crystals”, *Eng. Trans.*, 23, pp. 157-183, 1975.
- [TEO 76] TEODOSIU C., SIDOROFF F., “A finite theory of the elastoviscoplasticity of single crystals”, *Int. J. Eng. Sci.*, 14, pp. 713-723, 1976.

- [VER 98] VERDIER M., FIVEL M.C., GROMA I., “Mesoscopic scale simulation of dislocation dynamic in fcc metals: principle and applications”, *Modelling Simul. Mater. Sci. Eng.*, 6(6), pp. 755-770, 1998.
- [WEY 02] WEYGAND D., FRIEDMAN L.H., VAN DER GIESSEN E., NEEDLEMAN A., “Aspects of boundary-value problem solutions with three-dimensional dislocation dynamics”, *Modelling Simul. Mater. Sci. Eng.*, 10(3), pp. 437-468, 2002.
- [WIL 70] WILLIS J.R., “Stress fields produced by dislocations in anisotropic media”, *Phil. Mag.*, 21, pp. 931-949, 1970.
- [ZBI 98] ZBIB H. M., RHEE M., HIRTH J. P., “On plastic deformation 3D dislocations”, *Int. J. Mech. Sci.*, (2-3), pp. 113-127, 1998.